HHS Public Access

Author manuscript

NMR Biomed. Author manuscript; available in PMC 2022 October 17.

Published in final edited form as:

NMR Biomed. 2021 September ; 34(9): e4568. doi:10.1002/nbm.4568.

Brain metabolism in tau and amyloid mouse models of Alzheimer's disease: an MRI study

Zhiliang Wei[1,2,*], **Jiadi Xu**[1,2], **Lin Chen**[1,2,3], **Lydiane Hirschler**[4,5], **Emmanuel L. Barbier**[4], **Tong Li**[6], **Philip C. Wong**[6], **Hanzhang Lu**[1,2,7]

[1]Russell H. Morgan Department of Radiology and Radiological Science, Johns Hopkins University School of Medicine, Baltimore, Maryland, USA.

[2]F. M. Kirby Research Center for Functional Brain Imaging, Kennedy Krieger Research Institute, Baltimore, Maryland, USA.

[3]Department of Electronic Science, Fujian Provincial Key Laboratory of Plasma and Magnetic Resonance, Xiamen University, Xiamen, Fujian, China.

[4]Université Grenoble Alpes, Inserm, U1216, Grenoble Institut Neurosciences, Grenoble, France.

[5]C.J. Gorter Center for High Field MRI, Department of Radiology, Leiden University Medical Center, Leiden, The Netherlands

[6]Department of Pathology, Johns Hopkins University School of Medicine, Baltimore, Maryland, USA.

[7]Department of Biomedical Engineering, Johns Hopkins University School of Medicine, Baltimore, Maryland, USA.

Abstract

Alzheimer's disease (AD) is the leading cause of cognitive impairment and dementia in elder individuals. According to the current biomarker framework for "unbiased descriptive classification", biomarkers of neurodegeneration, "N", constitute a critical component in the tri-category "A/T/N" system. Current biomarkers of neurodegeneration suffer from potential drawbacks such as requiring invasive lumbar puncture, involving ionizing radiation, or representing a late, irreversible marker. Recent human studies have suggested that reduced brain oxygen metabolism may be a new functional marker of neurodegeneration in AD, but the heterogeneity and the presence of mixed pathology in human patients did not allow a full understanding of the role of oxygen extraction and metabolism in AD. In this report, global brain oxygen metabolism and related physiological parameters were studied in two AD mouse models with relatively pure pathology, using advanced MRI techniques including T_2-relaxation-under-spin-tagging (TRUST) and phase contrast (PC) MRI. Additionally, regional cerebral blood flow (CBF) was determined with pseudo-continuous arterial spin labeling (pCASL). Reduced global oxygen extraction fraction (OEF) (by −18.7%, P=0.008), unit-mass cerebral metabolic rate of oxygen ($CMRO_2$) (by −17.4%, P=0.04), and total $CMRO_2$ ($TCMRO_2$) (by −30.8%, P<0.001)

*Corresponding author: Zhiliang Wei, Ph.D., The Russell H. Morgan Department of Radiology and Radiological Science, Johns Hopkins University School of Medicine, 600 N. Wolfe Street, Park 340, Baltimore, MD 21287, zhiliang.wei@jhu.edu Phone: 443-453-2581.

were observed in a tau AD model, referred to as Tau4RΔK mice, that manifested pronounced neurodegeneration as measured by diminished brain volume (by −15.2%, P<0.001). Global and regional CBF in these mice were not different from those of wild-type mice (P>0.05), suggesting a normal vascular function. In contrast, in an amyloid AD model (B6;SJL-Tg(APPSWE)2576Kha), referred to as APP mice, that did not reveal brain volume reduction, relatively intact brain oxygen extraction and metabolism were found (P>0.05). Consistent with the imaging data, behavioral measures of walking distance were impaired in Tau4RΔK mice (P=0.004), but not in the APP mice (P=0.88). Collectively, these findings support the hypothesis that non-invasive MRI measurement of brain oxygen metabolism may be a promising biomarker of neurodegeneration in AD.

Keywords

cerebral blood flow; oxygen extraction fraction; cerebral metabolic rate of oxygen; TRUST; phase contrast; arterial spin labelling; Alzheimer's disease

INTRODUCTION

Alzheimer's disease (AD) is the leading cause of cognitive impairment and dementia in elder individuals.[1–3] A great deal of efforts has been made to the development of biomarkers, including imaging markers, for the diagnosis and treatment monitoring of this devastating disease.[4–7] There is a recent consensus to use these biomarkers for "unbiased descriptive classification".[8] In this scheme, rather than using the biomarkers to help label each individual as "normal", "MCI', or "dementia", Jack *et al.* proposed an "A/T/N" system in which major AD biomarkers are divided into 3 binary categories based on the nature of the pathophysiology each measures.[8] "A" refers to the value of a β-amyloid biomarker; "T" is the value of a phosphorylated tau biomarker; and "N" represents biomarkers of neurodegeneration or neuronal injury. At present, assessment of neurodegeneration (i.e., the "N") is based on [18F]-fluorodeoxyglucose-PET,[9] brain volume as measured by anatomic MRI,[10] or total tau determined from cerebrospinal fluid (CSF).[11] However, CSF sampling requires invasive lumbar puncture, PET involves ionizing radiation, and brain volume atrophy is a late, irreversible marker. Therefore, it is desirable to develop non-invasive and early biomarker of neurodegeneration.

Recent research in human patients has suggested that the brain's oxygen extraction fraction (OEF) and cerebral metabolic rate of oxygen ($CMRO_2$), even for a whole-brain measure, were reduced in patients with mild cognitive impairment (MCI).[12,13] This observation is consistent with the notion that the brain's oxygen consumption reflects the aggregated neural activity, thus neurodegeneration is expected to be accompanied by diminished energy and oxygen utilization. Moreover, cognitively normal carriers of the apolipoprotein E4 gene, which is a risk factor for AD, manifested lower global brain oxygen extraction when compared with non-carriers.[14] Another report revealed that lower OEF was associated with poorer cognitive scores.[15] Therefore, brain oxygen metabolism may provide a rapid and non-invasive functional biomarker for neurodegeneration in AD. However, human cognitive impairment and dementia often contain mixed pathological underpinnings,[16–19] such as amyloidosis, tauopathy, vascular, Parkinson's, and Lewy body conditions. Therefore, a study

in animal models with relatively pure pathology is critical to provide further understanding of the characteristic of brain metabolism in AD.

In this study, we performed global measurements of brain oxygen metabolism and its related parameters, i.e., OEF, total blood flow (TBF), unit-mass cerebral blood flow (CBF), total $CMRO_2$ ($TCMRO_2$), and unit-mass $CMRO_2$, with advanced physiological MRI techniques. Additionally, regional CBF was measured in the same mice. Two mouse models of AD were used. One is a tau transgenic model, referred to as the Tau4RΔK model,[20] which overexpresses the tau protein and reveals brain atrophy, thus representing a model that manifests both AD-related pathology and neurodegeneration. The other model is an amyloid transgenic model, referred to as amyloid-precursor-protein (APP) model, which mimics the deposition of amyloid plaques[21] in the absence of brain atrophy,[22,23] thereby representing a model in which AD pathology is present but neurodegeneration absent. In addition to imaging, behavior tests based on Y-maze[24,25] were performed as a measure of cognitive function and correlation between behavioral performances and MRI measures were studied.

EXPERIMENTAL

Animals

The experimental protocols involved in this study have been approved by the Johns Hopkins Medical Institute Animal Care and Use Committee and were conducted in accordance with the National Institutes of Health guideline for the care and use of laboratory animals. In one study (Study 1), a cohort of 9 Tau4RΔK mice (2 Male 7 Female, body weight: 26.4 ±3.1 grams, age: 52±4 weeks) and 11 wild-type (WT) littermates (C57BL/6 mice, 5 Male 6 Female, body weight: 31.3±6.4 grams, age: 50±2 weeks) was scanned. Body weight and age were described in the format of Mean ± Standard deviation. There was not a significant difference between Tau4RΔK and WT mice in age (P=0.32), although the Tau4RΔK mice showed a trend of lower body weight (P=0.054). Tau4RΔK mice were locally generated and bred as described previously.[20] Briefly, DNA fragments encoding ΔK280 mutant four-repeat domains of tau were microinjected into C57BL/6 X SJL F2 mouse embryos to produce transgenic mice carrying mutant Tau fragment with a regulatory element, moPrP-tetP promoter. Subsequently, these mice were crossbred with CamKII-tTA mice to bring the Tau transgene under the control of tet-off CamKII promoter62, resulting in Tau4RΔK mice.

In a separate study (Study 2), a cohort of 5 APP mice (B6;SJL-Tg(APPSWE)2576Kha mice, 5 Female, body weight: 22.2±1.8 grams) and 5 WT littermates (B6;SJL mice, 5 Female, body weight: 23.0±1.9 grams) purchased from Taconic Biosciences was scanned to collect the MRI data. Since the sample size of this cohort was smaller than the tau-mouse study, we performed the measurements at multiple time points, specifically at ages of 46, 51, and 56 weeks, in order to augment the statistical power. Due to the difference of genetic background between Tau4RΔK and APP cohorts, separate WT mice were used for the two studies.

All mice were genotyped before group assignment. In addition, the age of 50–52 weeks was chosen for the current study due to findings of neurofibrillary tangles and amyloid plaques in Tau4RΔK[20] and APP[21] mice, respectively, at an age of approximately 12 months in previous

reports. All mice had free access to food and water, and were housed in groups (N<5 per cage without cage enrichment) in a quiet environment with a 12h day/night cycle.

MRI Experiments

All MRI experiments were performed on an 11.7T Bruker Biospec system (Bruker, Ettlingen, Germany) equipped with a horizontal bore and actively shielded pulsed field gradients (maximum intensity of 0.74 T/m). Within each study, the order of receiving MRI scan for each mouse was randomized. Mice were first pre-assigned to consecutive numbers from one. The MATLAB (MathWorks, Natick, MA) “rand” function was then used to generate an array of pseudorandom numbers. The ranks of these numbers (largest to smallest) were used to determine the experimental orders (e.g. if the first pseudorandom number ranked 5^{th} in the array, the mouse pre-assigned to number 5 was the first one to be scanned). Group information was not blinded when running the experiment or processing the data.

Images were acquired using a 72-mm quadrature volume resonator as transmitter, and a four-element (2×2) phased-array coil as receiver. The B_0 field over the mouse brain was shimmed with a global shimming scheme (up to 2^{nd} order) based on a subject-specific pre-acquired field map. Anesthesia was carried by regular air (21% O_2, 78% N_2) with 1.5% vaporized isoflurane for 15 min as induction, then 1.0% for maintenance until the end of experiments. Respiration rate was monitored during the experiment to ensure the survival of the mouse. In case that a mouse breathed at a rate >150 breaths per minute, the maintenance isoflurane dosage was increased slightly to ~1.2%. For MRI scanning, the mouse was immobilized with a bite bar and ear pins and then placed on a water-heated animal bed with temperature control.

MRI assessment of brain physiology consisted of global measurements of brain volume, TBF, CBF, OEF, $TCMRO_2$, and $CMRO_2$, as well as regional measurement of CBF.

OEF is defined as the arteriovenous difference in blood oxygenation, i.e., $OEF=Y_a-Y_v$. The arterial oxygenation (Y_a) is generally characterized by a narrow dynamic range and close to unity (assumed to be 0.99).[26,27] Global venous oxygenation (Y_v) was assessed by a TRUST MRI technique, which was first developed on human scanners,[28,29] and recently optimized and utilized at animal MRI systems.[30–32] Specifically, an axial time-of-flight (TOF) sequence was first performed to visualize the confluence of sagittal sinuses, with the following parameters: TR/TE = 20/2.6 ms, field of view (FOV) = 16×16 mm^2, matrix size = 256×256, 35 axial slices, slice thickness = 0.5 mm, and scan duration = 2.2 min. The TRUST scan was then positioned to intersect the confluences of sagittal sinuses based on the TOF images, and was repeated three times to improve reliability. TRUST MRI was performed with the following parameters: TR/TE = 3500/6.5 ms, FOV = 16×16 mm^2, matrix size = 128×128, slice thickness = 0.5 mm, EPI factor = 16, inversion-slab thickness = 2.5 mm, post-labeling delay = 1000 ms, eTE = 0.25, 20, 40 ms, echo spacing of eTE = 5.0 ms, and scan duration = 2.8 min.

Whole-brain TBF and CBF were evaluated with PC MRI. TBF (in ml/min) was defined as the total amount of blood flowing into the brain per unit time, which was estimated

by the summation of blood flows in four major feeding arteries, i.e. left internal carotid artery (LICA), right internal carotid artery (RICA), left vertebral artery (LVA), and right vertebral artery (RVA).[33] Four PC MRI scans were performed with each corresponding to one artery. Prior to the PC scans, we performed a coronal TOF angiogram (7 slices, slice thickness = 0.5 mm, no inter-slice gap, TR/TE = 45/2.6 ms, scan duration = 2.0 min) to visualize the feeding arteries. Next, a sagittal TOF (single slice, tilted to contain the target artery identified from coronal TOF images, thickness = 0.5 mm, TR/TE = 60/2.5 ms, scan duration = 0.4 min) was applied to visualize the in-plane trajectory of the targeted artery. PC MRI was then positioned using both TOFs and performed using following parameters: TR = (Study 1) 15ms / (Study 2) 60 ms, TE=3.2 ms, FOV = (Study 1) 15×10 / (Study 2) 15×15 mm^2, matrix size = (Study 1) 300×200 / (Study 2) 300×300, slice thickness = 0.5 mm, number of average = 4, dummy scan = 8, receiver bandwidth = 100 kHz, flip angle = 25°, partial Fourier acquisition factor = 0.7, and scan duration = (Study 1) 0.4 min / (Study 2) 2.4 min. Unit-mass CBF (in ml/100g/min) was obtained by normalizing TBF by brain weight, which can be evaluated from a T_2-weighted fast-spin-echo MRI protocol (TR/TE = 4000/26 ms, FOV = 15×15 mm^2, matrix size = 128×128, slice thickness = 0.5 mm, echo spacing = 5 ms, 35 axial slices, and scan duration = 1.1 min). Tissue density was assumed to be 1.04 g/ml.[34]

Unit-mass $CMRO_2$ was computed from OEF and CBF using the Fick principle,[35–37] i.e., $CMRO_2 = C_a \cdot OEF \cdot CBF$, where C_a denotes the molar concentration of oxygen in a unit volume of fully oxygenated blood and was assumed to be 882.1 μmol O_2/100 ml blood based on previous literature[38,39]. $CMRO_2$ is written in the unit of μmol oxygen per 100 g brain tissue per min (μmol O_2/100g/min). Similarly, $TCMRO_2$ (in μmol O_2/min) can be calculated without normalization to the brain weight.

In addition to the above whole-brain measures, regional CBF was evaluated with pCASL MRI[40,41] in Study 1. A two-scan pCASL scheme[42,43] was utilized to improve its robustness against residual magnetic-field inhomogeneity at the high field (11.7T). The experimental parameters were: TR/TE = 3000/16.6 ms, FOV = 15×15 mm^2, matrix size = 96×96, slice thickness = 1.0 mm, labeling-pulse width = 0.4 ms, inter-labeling-pulse delay = 0.8 ms, mean B_1 amplitude = 2.5 μT, labeling duration = 2000 ms, post-labeling delay = 400 ms, receiver bandwidth = 300 kHz, number of average = 25, partial Fourier acquisition factor = 0.7, slice number = 9, and scan duration = 2.5 min.

At the end of the MRI session, two or three drops of blood were collected using the submandibular bleeding method[44] in each mouse outside the scanner when mouse was still in narcosis state. The blood was used to measure the hematocrit (Hct) level of the mouse with a HemoCue Hb 201^+ system (HemoCue AB, Angelholm, Sweden). Measurements were repeated three times and an average value was obtained.

Behavior test was performed in each mouse after its final MRI session but on a different day to minimize fatigue. A Y-maze with three equidistant identical arms was used to assess the spatial memory of tested mice.[25,45] Different mice were tested in a randomized order and from a randomized starting arm. Each Y-maze session lasted 5 min. The walking track of each mouse was recorded by a camera within its 5-min session, and total walking distance

was calculated by summing up the length of walking track. After placed in the Y-maze, mice generally explored the least recently visited arm and thus tended to alternate their visit among the three arms.[45] A spontaneous alternation was defined as successive entries into the three different arms. Denoting the arms as A, B, and C, a spontaneous alternation can be ABC, BCA, CAB, BAC, ACB, or CBA. Spontaneous alternating performance (SAP) was defined as the ratio between the number of spontaneous alternating and the number of total alternations.[45]

Data Processing

Data processing of TRUST MRI was conducted with a custom-written graphic-user-interface (GUI) tool built on MATLAB and followed procedures detailed previously[28,30]. Briefly, for each TRUST dataset, subtraction between the control and labeled images was performed to obtain difference images (Figure 1a). A region of interest (ROI) was manually drawn on the difference image to encompass the sinus confluence. Four voxels within the ROI with the largest difference signals were selected for spatial averaging. Then, venous blood signal intensities at three different eTE values were fitted into a monoexponential function to obtain T_2 (Figure 1a). Finally, T_2 was converted into Y_v using a T_2-Y_v calibration plot (Figure 1a) reported by Li et al.[46]. The measured Hct of individual mouse was used in the conversion.

Processing of the PC dataset followed steps described in a previous report.[33] The artery of interest was first manually delineated on the complex-difference image (Figure 1b), which shows an excellent contrast between vessel and surrounding tissue. The mask was then applied to the velocity map and the integration of arterial voxels yields blood flow through that artery in ml/min. To estimate brain volume, the T_2-weighted images were analyzed manually by delineating the brain boundary on a slice-by-slice basis while referencing to a mouse brain atlas (https://atlas.brain-map.org/).[32] Voxels inside the masks were summed to yield the total brain volume in mm^3. The total brain volume was used in the estimation of unit-mass CBF.

For the processing of the pCASL dataset, pair-wise subtraction between control and labeled images ($M_{ctr} - M_{lbl}$) were first applied to yield a difference image, which was then divided by a M_0 image to provide a perfusion index image, i.e., $CBF_{index} = (M_{ctr} - M_{lbl})/M_0$, where M_0 was calculated from the control image[42] and by assuming a tissue T_1 of 1900 ms[47]. Since it is difficult to determine the inversion efficiency of pCASL labelling in mice, a normalization method[48] based on global CBF (from PC MRI) was used to obtain absolute CBF maps. Specifically, i.e., $CBF_{pCASL} = CBF_{index}/Mean(CBF_{index}) \cdot CBF_{PC}$. ROIs were manually drawn to encompass cortex, hippocampus, thalamus, and striatum, by referring to the mouse brain atlas (https://atlas.brain-map.org/). Voxel-wise CBF values within each ROI were averaged to estimate the perfusion of the corresponding region.

Statistical analyses

In Study 1, a multi-linear regression model was used to study the effect of mouse group (i.e. Tau4RΔK versus WT) on physiological and anatomical MRI parameters, in which the MRI parameters were the dependent variables. Mouse group and sex were used as the

independent variables. In Study 2, a linear mixed-effect model (fixed terms for the group effect and time effect, and a random term for different mice) was used to analyze the multi-time-point dataset of APP and WT mice. A P value of 0.05 or less is considered significant.

RESULTS

Figure 1a shows representative data of TRUST MRI, including control and labeled images as well as a difference image highlighting pure venous-blood signal (at eTE=0.25 ms as an example). Signal intensities of venous blood were then fitted to a monoexponential function to estimate the venous T_2, which was converted to Y_v with a Hct-T_2-Yv calibration plot[46]. Figure 1b presents the complex-difference images and velocity maps of PC MRI in the four major feeding arteries (LICA, RICA, LVA, and RVA). The ROIs drawn on the complex-difference images are also shown. Figure 1c displays pCASL images from a representative slice, including control, labeled, and perfusion image. Figure 1d shows a diagram summarizing how physiological parameters reported in this study were obtained from different MRI scans. Brain volume, TBF, OEF, $TCMRO_2$, and $CMRO_2$ were global measures, while CBF was measured in both global and regional fashions.

Tau4RΔK mouse study. Figure 2 summarizes the MRI results of the Tau4RΔK study. Tau4RΔK mice were found to have a smaller brain volume (Figure 2a, P<0.001), smaller TBF (Figure 2b, P=0.02), similar unit-mass CBF (Figure 2c, P=0.99), lower OEF (Figure 2d, P=0.008), smaller $TCMRO_2$ (Figure 2e, P<0.001), and smaller unit-mass $CMRO_2$ (Figure 2f, P=0.04), when compared with the WT mice. Additionally, venous T_2 values, from which OEF was derived, were 21.4±1.2 (mean ± standard error, N=11) and 25.8±1.5 ms (N=9) for the WT and Tau4RΔK mice (P=0.01), respectively. Sex did not show a significant effect in any of these parameters (P>0.05, see Table S1 in supporting information). Sex-by-group interaction effect was also insignificant (P>0.05). In terms of the magnitude of the differences, brain volume changed by −15.2%, TBF by −14.9%, OEF by −18.7%, $TCMRO_2$ by −30.8%, and unit-mass $CMRO_2$ by −17.4%. For regional CBF (Figure 2g), there were no differences in cortex (P=0.14), hippocampus (P=0.28), thalamus (P=0.50), and striatum (P=0.74).

Figure 3 shows the behavioral performances of the Tau4RΔK cohort, and correlations between behavioral performance and MRI measures. There was a significant difference in walking distance (Figure 3a, P=0.004) between Tau4RΔK and WT mice. The comparison of SAP scores between Tau4RΔK and WT mice was not significant (P=0.74). There was a trend of correlation between walking distance and OEF (Figure 3c, P=0.055). There was a correlation between walking distance and $TCMRO_2$ (Figure 3d, P=0.008). There were no relationships (P>0.05) between walking distance and other MRI measures.

The Hct levels were 42.0±2.6% (Mean ± Standard error) and 41.0±1.1% for the Tau4RΔK and WT mice, respectively, without a significant difference (P=0.83). We also tested to use an assumed Hct level (42.0%) for all mice in the T_2-Y_v calibration and found that the results were similar to those using Hct-specific calibration. Specifically, significant differences

between Tau4RΔK and WT mice were observed in OEF (P=0.01), $TCMRO_2$ (P<0.001) and unit-mass $CMRO_2$ (P=0.02).

APP mouse study.

Figure 4 summarizes the results of the APP mouse study. The linear mixed-effect model revealed that there was a significant difference in brain volume (Figure 4a, P=0.04) with the APP mice exhibiting larger brain volume compared with the WT mice. The APP mice showed similar TBF (Figure 4b, P=0.29), unit-mass CBF (Figure 4c, P=0.14), OEF (Figure 4d, P=0.78), $TCMRO_2$ (Figure 4e, P=0.42), and unit-mass $CMRO_2$ (Figure 4f, P=0.20) in comparison with their WT littermates. Similarly, walking distance (P=0.88) and SAP score (P=0.34) were not different between the APP and WT groups. There was not a time effect (P>0.05) on any of the MRI measures, presumably due to the relatively short time intervals used in this study.

DISCUSSION

To the best of our knowledge, this study is the first report to investigate the relationship between brain oxygen metabolism and AD in mouse models. Our main finding is that, in the AD mouse model that manifests neurodegeneration (i.e., with brain volumetric atrophy), oxygen extraction and total brain metabolism were diminished. On the other hand, in the AD mouse model that shows AD pathology but does not exhibit neurodegeneration, the brain's oxygen extraction and metabolism were unchanged. These evidences support the brain oxygen extraction and metabolism as a potential biomarker for neurodegeneration in AD.

Aerobic metabolism is the primary form of energy production in the brain. A majority of this energy budget is used to support neural activity.[49] Therefore, it is logical to expect that there is a good correspondence between aggregated neural activity and oxygen consumption and that oxygen metabolism can be used as a surrogate marker for neurodegeneration. However, measurement of oxygen metabolism has been technically challenging. The gold-standard technique is ^{15}O-based PET which requires three radiotracers in combination with the sampling of arterial blood.[50] Due the complexity of this technique, it has not been widely used in AD or other neurological diseases. Recent advances in MRI technology have allowed non-invasive and rapid measurements of oxygen extraction fraction and metabolism on clinical MRI scanners,[36,51–59] providing a new opportunity to examine the utility of oxygen metabolism as a candidate biomarker in AD. Previous human studies have provided evidences that OEF and $CMRO_2$ can differentiate between patient populations and was correlated with cognitive function.[12,14,15] However, the associations between oxygen metabolism and major hallmarks of AD, e.g. amyloid, tau, and neuron death, have not been elucidated and, due to the presence of mixed pathology in human patients, definitive determination is not trivial. Therefore, the present study provides important evidence on the potential of $OEF/CMRO_2$ as a neurodegeneration marker in the A/T/N classification system and, given the readiness of these techniques in human studies, may facilitate a broader clinical use of $OEF/CMRO_2$ MRI in dementia research and clinical management.

The hypometabolism found in the Tau4RΔK model is consistent with previous ^{18}F-FDG PET studies in other tau models.[60,61] The hTau model, which expressed six human tau isoforms, exhibited metabolic decline at ~14 months old,[60] and the 3xTg model, which was a mixed model harboring APP, PS1, and tau mutations, exhibited regional hypometabolism in cortical piriform and insular regions at 11 months old.[61] The vascular function of Tau4RΔK mice seems to be relatively intact, as the unit-mass CBF was not different from the WT mice. Moreover, there did not appear to be local perfusion alterations in the four major brain regions investigated, suggesting the absence of regional vascular impairment in this mouse model. There was a significant reduction in TBF (reduced by −14.9%), which was primarily attributed to the smaller brain volume in Tau4RΔK mice (by −15.2%). The finding of unaltered unit-mass CBF in Tau4RΔK model was consistent with the report in another tau transgenic model rTg4510.[62] In contrast, a report in the PS19 (also known as P301S) tau model revealed a small reduction in resting cortical and hippocampal CBF.[63] This discrepancy may be partly due to model differences. The PS19 model showed clasping and limb retraction when lifted by the tail at an early age of 3 months old, which progressively developed into hunched backs and then paralyses. As a result, approximately 80% mice died by 12 months with a median survival of ~9 months.[64] However, in rTg4510 mice, only the most severely affected mice exhibited hunched posture with hind-limb dysfunction at ~10 months old, and it was common for an rTg4510 mouse to live up to 16 months old,[65] suggesting that tau models can differ in the severity of pathology. Similarly, the Tau4RΔK mice used in the present study also has a longer survival time compared to the PS19 model. Therefore, it is possible that CBF alteration likely occurs in more aggressive tau AD models. In addition, it is interesting to note that our findings of a reduced brain metabolism with preserved unit-mass CBF mirrors the results in human MCI patients[12].

In contrast, the APP mice, despite the accumulation of amyloid plaques,[21] did not show brain volume reductions in comparison with their littermates, which is consistent with other reports on amyloid mouse model[22,23]. Accordingly, neither their oxygen extraction nor metabolism shows a reduction, suggesting that oxygen consumption is relatively intact in the absence of neurodegeneration. Combining the findings in the Tau4RΔK and APP studies, it can be hypothesized that abnormalities in brain oxygen metabolism, especially OEF and $CMRO_2$, are associated with the presence of neurodegeneration in AD, providing evidence that brain oxygen metabolism may be a functional biomarker for neurodegeneration.

The differential effects of amyloid and tau on brain metabolism and neurodegeneration observed in this study are generally consistent with the current mechanistic models of AD pathogenesis.[20,66] It is thought that amyloid plaque is necessary to provide a molecular environment to facilitate the biochemical modification of wild-type tau within dystrophic neurites. However, amyloid plaque alone is insufficient to convert the wild-type tau to a pathological conformation that drives neurodegeneration and cognitive decline. A second-risk determinant (e.g. tau fragmentation) will be required to drive the pathological conversion of wild-type tau. This “two-hit” hypothesis explains the phenomenon that subsets of individuals with amyloid plaques stayed cognitively normal[67] because they failed to harbor a “second-risk determinant” to drive the tau conversion. This hypothesis is consistent with the long pre-symptomatic phase of AD during which amyloid plaques accumulate

but tau remains unconverted due to the lack of another risk determinant. Moreover, this hypothesis supports the notion that neurodegeneration is more closely related to tau pathology than to amyloid plaques. The tau aggregate, which is a later event than amyloid plaque, is sufficient to propagate and spread throughout the brain via neuronal circuits and result in neuronal loss, neurodegeneration, and cognitive decline. Since brain oxygen metabolism reflects the amount of aggregated neural activity in the brain, OEF and $CMRO_2$ may be a surrogate marker for neurodegeneration in AD, although biological underpinnings on the molecular level, e.g. association between potential mitochondrial dysfunction and neurodegeneration, remain to be investigated in future studies.

As a technical consideration, the present study observed that the Tau4RΔK mice had a smaller brain volume after adjusting for sex. However, there was also a trend of lower body weight in the Tau4RΔK mice when compared with the WT mice. To account for the influence of body weight on brain volume and to rule out the possibility that the smaller brain volume is due to systemic malnutrition in the Tau4RΔK mice, we performed an additional analysis by including body weight in the statistical model. We found that the group effect remained significant, suggesting that brain atrophy observed in present study was not a result of body weight difference.

The influence of gray and white matter tissue composition on the measured physiological parameters was also considered. Previous studies using PET have shown that OEF is homogeneous across gray and white matters,[68] thus a change in the gray and white matter tissue composition is not expected to have an effect on whole-brain OEF. On the other hand, $CMRO_2$ is known to be higher in the gray than white matter. Thus, a reduced whole-brain-averaged $CMRO_2$ observed in the Tau4RΔK mice should be interpreted in the context of gray and white matter volume fractions. To investigate this issue, we studied atrophy rate in gray and white matter, and found that the atrophy in the cortex and corpus callosum of the Tau4RΔK mice were 18.2% and 22.6%, respectively. Thus it appears that volumetric loss occurred in both gray and white matter. Thus, the observed $CMRO_2$ change is not a consequence of changes in gray and white matter brain volume.

Since our TRUST scan had three repetitions, we were able to obtain a precision index of the T_2 estimation (calculated as standard deviation across repetitions divided by square root of repetition number), which was found to be 1.5±0.2 ms (N=20). This is smaller than the T_2 differences (4.4 ms) between mouse groups. Therefore, OEF difference between Tau4RΔK and littermate WT mice was primarily attributed to the model pathology rather than physiological noise or methodological variance. However, since TRUST MRI is a global measure of oxygen extraction, it cannot pinpoint the spatial location or distribution of the OEF reduction. In fact, a potential arterio-venous shunting in the presence of normal tissue OEF may also result in a TRUST alteration. Future studies using localized OEF techniques such as T_2-relaxation-under-phase contrast (TRUPC) MRI,[69] quantitative susceptibility mapping (QSM),[70] or quantitative BOLD[71] methods may prove valuable in further characterizing OEF abnormalities in AD.

The vasoactive effect of isoflurane on physiological parameters[72] may be one potential confounding factor in animal studies like ours. Therefore, in current study, a consistent

anesthetic regimen, which has been shown to be helpful in mitigating anesthetic effects over different experimental sessions,[32] was used throughout this study. With this strategy, while the absolute values of physiological parameters may not be directly comparable to unanesthetized state, comparisons between groups under a consistent anesthetic regimen are expected to be valid.

To provide an assessment of the power of our studies, power calculations were performed by Monte-Carlo simulations (2000 iterations) based on the target of detecting a 20% group-level difference in physiological parameters. For the Tau4RΔK study with a sample size of 11 for WT and 9 for Tau4RΔK mice, we have a power of 78%, 63%, 80%, 74%, and 60% to detect a significant effect in TBF, CBF, OEF, $TCMRO_2$, and $CMRO_2$ at $P<0.05$, respectively. For the APP study with a sample size of 5 in both WT and APP groups and three time points in each animal, we have a power of 76%, 74%, 92%, 83%, and 84% to detect a significant effect in TBF, CBF, OEF, $TCMRO_2$, and $CMRO_2$, respectively. These power values support the study design in present report.

Results of this study should be interpreted in the context of several limitations. First, the sample size of APP cohort is relatively small (N=5 for each group). In order to enhance the statistical power of data, we performed the experiments in a longitudinal fashion to increase the number of total experimental sessions and analyzed the data with an advanced statistical model (linear mixed-effect model). Second, histological results were not included in the present report. We performed verifications of AD pathologies and neuron counts in representative animals to confirm the mouse models (see Figure S1 in supporting information), but did not conduct histology in all animals. Note, however, that histological results of these mouse models have been reported extensively in previous literatures of the corresponding models.[20,21] In the previous report on Tau4RΔK mice,[20] histology analyses at multiple ages, i.e., 6, 9, 12, and 18 months, revealed that: (i) brain weight of Tau4RΔK mice showed progressive age-dependent reduction in unison with size decreases in hippocampus and cortex; (ii) there was a marked reduction of neuron numbers by 12 months old, e.g., in CA1, CA2&CA3 regions (as also shown by the cresyl violet staining in supporting Figures S1a&S1b); (iii) tau tangles first appeared at 6 months old, and then dramatically increased by 12 months old. Regarding the APP mice used in current study, Hsiao et al. reported extracellular amyloid deposits as a result of over-expressing the 695-amino acid isoform of human β-amyloid precursor protein at 12 months old[21] (as also shown by the 6E10 staining in supporting Figures S1c&S1d). Those histology findings were consistent with the major hallmarks of human AD patients, namely, neurofibrillary tangles and amyloid plaques. Thirdly, there was a lack of gender balance in Study 2. Future studies that include both male and female APP mice are needed to confirm our findings. Finally, we only performed studies in two mouse models of AD but did not explore other types of AD mice, for example, those that develop both tau tangles and amyloid plaques. Such experiments will prove helpful in understanding the interaction of amyloid and tau in affecting neurodegeneration in AD, and should be pursued in future studies.

CONCLUSIONS

Brain oxygen metabolism was studied in two mouse models of Alzheimer's disease. Reduced oxygen extraction fraction and metabolism was observed in a tau model that manifested pronounced neurodegeneration as measured by brain volume. In contrast, relatively intact brain oxygen extraction and metabolism were found in an amyloid model that did not reveal neurodegeneration. Collectively, these findings support the hypothesis that non-invasive MRI measurement of brain oxygen metabolism may be a promising biomarker of neurodegeneration in AD.

Supplementary Material

Refer to Web version on PubMed Central for supplementary material.

ACKNOWLEDGEMENTS

This work was supported by the grant sponsors of NIH R21 AG058413, NIH R01 NS106702, NIH R01 NS106711, NIH R01 AG064792, NIH RF1 AG071515, NIH R01 MH084021, and NIH P41 EB015909.

DATA AVAILABILITY STATEMENT

The datasets used in this study are available upon request to the corresponding author.

Abbreviations

AD	Alzheimer's disease
APP	amyloid precursor protein
CBF	cerebral blood flow
$CMRO_2$	cerebral metabolic rate of oxygen
CSF	cerebrospinal fluid
FOV	field of view
LICA	left internal carotid artery
LVA	left vertebral artery
MCI	mild cognitive impairment
OEF	oxygen extraction fraction
PC	phase contrast
pCASL	pseudo-continuous arterial spin labeling
RICA	right internal carotid artery
ROI	region of interest

RVA	right vertebral artery
SAP	spontaneous alternating performance
TBF	total blood flow
$TCMRO_2$	total cerebral metabolic rate of oxygen
TOF	time of flight
TRUST	T_2-relaxation-under-spin-tagging
Y_a	arterial oxygenation
Y_v	venous oxygenation

REFERENCES

1. Rizzi L, Rosset I, Roriz-Cruz M. Global epidemiology of dementia: Alzheimer's and vascular types. Biomed Res Int 2014; 2014: 908915.
2. Alzheimer's Association, 2020 Alzheimer's disease facts and figures. Alzheimers Dement 2020; 16: 391–460.
3. Nichols E, Szoeke CEI, Vollset SE et al. Global, regional, and national burden of Alzheimer's disease and other dementias, 1990–2016: a systematic analysis for the Global Burden of Disease Study 2016. The Lancet Neurology 2019; 18(1): 88–106. [PubMed: 30497964]
4. Blennow K, Zetterberg H. Biomarkers for Alzheimer's disease: current status and prospects for the future. J Intern Med 2018; 284(6): 643–663. [PubMed: 30051512]
5. Khoury R, Ghossoub E. Diagnostic biomarkers of Alzheimer's disease: A state-of-the-art review. Biomarkers in Neuropsychiatry 2019; 1: 100005.
6. Zetterberg H, Bendlin BB. Biomarkers for Alzheimer's disease-preparing for a new era of disease-modifying therapies. Mol Psychiatry 2020; DOI: 10.1038/s41380-020-0721-9.
7. Falangola MF, Jensen JH, Tabesh A et al. Non-Gaussian diffusion MRI assessment of brain microstructure in mild cognitive impairment and Alzheimer's disease. Magn Reson Imaging 2013; 31(6): 840–6. [PubMed: 23602730]
8. Jack CR Jr., Bennett DA, Blennow K et al. A/T/N: An unbiased descriptive classification scheme for Alzheimer disease biomarkers. Neurology 2016; 87(5): 539–547. [PubMed: 27371494]
9. Khosravi M, Peter J, Wintering NA et al. 18F-FDG Is a Superior Indicator of Cognitive Performance Compared to 18F-Florbetapir in Alzheimer's Disease and Mild Cognitive Impairment Evaluation: A Global Quantitative Analysis. J Alzheimers Dis 2019; 70(4): 1197–1207. [PubMed: 31322568]
10. Bartos A, Gregus D, Ibrahim I et al. Brain volumes and their ratios in Alzheimer s disease on magnetic resonance imaging segmented using Freesurfer 6.0. Psychiatry Res Neuroimaging 2019; 287: 70–74. [PubMed: 31003044]
11. Blennow K, Wallin A, Agren H et al. Tau protein in cerebrospinal fluid: a biochemical marker for axonal degeneration in Alzheimer disease? Mol Chem Neuropathol 1995; 26(3): 231–245. [PubMed: 8748926]
12. Thomas BP, Sheng M, Tseng BY et al. Reduced global brain metabolism but maintained vascular function in amnestic mild cognitive impairment. J Cereb Blood Flow Metab 2017; 37(4): 1508–1516. [PubMed: 27389176]
13. Liu J, Zhu YS, Khan MA et al. Global brain hypoperfusion and oxygenation in amnestic mild cognitive impairment. Alzheimers Dement 2014; 10(2): 162–170. [PubMed: 23871763]
14. Lin Z, Sur S, Soldan A et al. Brain Oxygen Extraction by Using MRI in Older Individuals: Relationship to Apolipoprotein E Genotype and Amyloid Burden. Radiology 2019; 292(1): 140–148. [PubMed: 31012816]

15. Jiang D, Lin Z, Liu P et al. Brain Oxygen Extraction Is Differentially Altered by Alzheimer's and Vascular Diseases. J Magn Reson Imaging 2020; 52(6): 1829–1837. [PubMed: 32567195]
16. Fernando MS, Ince PG, Function MRCC et al. Vascular pathologies and cognition in a population-based cohort of elderly people. J Neurol Sci 2004; 226(1–2): 13–17. [PubMed: 15537512]
17. Schneider JA, Arvanitakis Z, Bang W et al. Mixed brain pathologies account for most dementia cases in communitydwelling older persons. Neurology 2007; 69: 2197–2204. [PubMed: 17568013]
18. Schneider JA, Wilson RS, Bienias JL et al. Cerebral infarctions and the likelihood of dementia from Alzheimer disease pathology. Neurology 2004; 62: 1148–1155. [PubMed: 15079015]
19. Esiri MM, Nagy Z, Smith MZ et al. Cerebrovascular disease and threshold for dementia in the early stages of Alzheimer's disease. Lancet 1999; 354(9182): 919–920. [PubMed: 10489957]
20. Li T, Braunstein KE, Zhang J et al. The neuritic plaque facilitates pathological conversion of tau in an Alzheimer's disease mouse model. Nat Commun 2016; 7: 12082.
21. Hsiao K, Chapman P, Nilsen S et al. Correlative memory deficits, Abeta elevation, and amyloid plaques in transgenic mice. Science 1996; 274(5284): 99–102. [PubMed: 8810256]
22. von Kienlin M, Kunnecke B, Metzger F et al. Altered metabolic profile in the frontal cortex of PS2APP transgenic mice, monitored throughout their life span. Neurobiol Dis 2005; 18(1): 32–39. [PubMed: 15649694]
23. Maheswaran S, Barjat H, Rueckert D et al. Longitudinal regional brain volume changes quantified in normal aging and Alzheimer's APP x PS1 mice using MRI. Brain Res 2009; 1270: 19–32. [PubMed: 19272356]
24. Hakimizadeh E, Jandaghi F, Hajmohammadi M et al. Pistachio extract improves neurocognitive behaviors in ovariectomized mice. Res J Pharmacogn 2019; 6: 45–51.
25. Liu N, Wang Y, An AY et al. Single housing-induced effects on cognitive impairment and depression-like behavior in male and female mice involve neuroplasticity-related signaling. Eur J Neurosci 2020; 52(1): 2694–2704. [PubMed: 31471985]
26. Lu H, Xu F, Rodrigue KM et al. Alterations in cerebral metabolic rate and blood supply across the adult lifespan. Cereb Cortex 2011; 21(6): 1426–1634. [PubMed: 21051551]
27. Li M, Ratcliffe SJ, Knoll F et al. Aging: impact upon local cerebral oxygenation and blood flow with acute isovolemic hemodilution. J Neurosurg Anesthesiol 2006; 18(2): 125–131. [PubMed: 16628066]
28. Lu H, Ge Y. Quantitative evaluation of oxygenation in venous vessels using T2-Relaxation-Under-Spin-Tagging MRI. Magn Reson Med 2008; 60(2): 357–363. [PubMed: 18666116]
29. Lu H, Xu F, Grgac K et al. Calibration and validation of TRUST MRI for the estimation of cerebral blood oxygenation. Magn Reson Med 2012; 67(1): 42–49. [PubMed: 21590721]
30. Wei Z, Xu J, Liu P et al. Quantitative assessment of cerebral venous blood T2 in mouse at 11.7T: Implementation, optimization, and age effect. Magn Reson Med 2018; 80(2): 521–528. [PubMed: 29271045]
31. Wei Z, Wang Q, Modi HR et al. Acute-stage MRI cerebral oxygen consumption biomarkers predict 24-hour neurological outcome in a rat cardiac arrest model. NMR Biomed 2020: e4377. [PubMed: 32662593]
32. Wei Z, Chen L, Hou X et al. Age-related alterations in brain perfusion, venous oxygenation, and oxygen metabolic rate of mice: A 17-month longitudinal MRI study. Front Neurol 2020; 11: 559. [PubMed: 32595596]
33. Wei Z, Chen L, Lin Z et al. Optimization of phase-contrast MRI for the estimation of global cerebral blood flow of mice at 11.7T. Magn Reson Med 2019; 81(4): 2566–2575. [PubMed: 30393888]
34. Leithner C, Muller S, Fuchtemeier M et al. Determination of the brain-blood partition coefficient for water in mice using MRI. J Cereb Blood Flow Metab 2010; 30(11): 1821–1824. [PubMed: 20842161]
35. Kety SS, Schmidt CF. The nitrous oxide method for the quantitative determination of cerebral blood flow in man: Theory, procedure and normal values. J Clin Invest 1948; 27(4): 476–483. [PubMed: 16695568]

36. Bulte DP, Kelly M, Germuska M et al. Quantitative measurement of cerebral physiology using respiratory-calibrated MRI. Neuroimage 2012; 60(1): 582–591. [PubMed: 22209811]
37. Xu F, Ge Y, Lu H. Noninvasive quantification of whole-brain cerebral metabolic rate of oxygen (CMRO2) by MRI. Magn Reson Med 2009; 62(1): 141–148. [PubMed: 19353674]
38. Ulatowski JA, Oja JME, Suarez JI et al. In vivo determination of absolute cerebral blood volume using hemoglobin as a natural contrast agent: An MRI study using altered arterial carbon dioxide tension. J Cereb Blood Flow Metab 1999; 19: 809–817. [PubMed: 10413037]
39. Chong SP, Merkle CW, Leahy C et al. Cerebral metabolic rate of oxygen (CMRO2) assessed by combined Doppler and spectroscopic OCT. Biomed Opt Express 2015; 6(10): 3941–3951. [PubMed: 26504644]
40. Dai W, Garcia D, de Bazelaire C et al. Continuous flow-driven inversion for arterial spin labeling using pulsed radio frequency and gradient fields. Magn Reson Med 2008; 60(6): 1488–1497. [PubMed: 19025913]
41. Alsop DC, Detre JA, Golay X et al. Recommended implementation of arterial spin-labeled perfusion MRI for clinical applications: A consensus of the ISMRM perfusion study group and the European consortium for ASL in dementia. Magn Reson Med 2015; 73(1): 102–116. [PubMed: 24715426]
42. Hirschler L, Debacker CS, Voiron J et al. Interpulse phase corrections for unbalanced pseudo-continuous arterial spin labeling at high magnetic field. Magn Reson Med 2018; 79(3): 1314–1324. [PubMed: 28585234]
43. Hirschler L, Munting LP, Khmelinskii A et al. Transit time mapping in the mouse brain using time-encoded pCASL. NMR Biomed 2018; 31: e3855.
44. Golde WT, Gollobin P, Rodriguez LL. A rapid, simple, and humane method for submandibular bleeding of mice using a lancet. Lab Anim (NY) 2005; 34(9): 39–43.
45. Mandillo S, Tucci V, Holter SM et al. Reliability, robustness, and reproducibility in mouse behavioral phenotyping: a cross-laboratory study. Physiol Genomics 2008; 34(3): 243–255. [PubMed: 18505770]
46. Li W, van Zijl PCM. Quantitative theory for the transverse relaxation time of blood water. NMR Biomed 2020: e4207. [PubMed: 32022362]
47. Ahrens ET, Dubowitz DJ. Peripheral somatosensory fMRI in mouse at 11.7 T. NMR Biomed 2001; 14(5): 318–324. [PubMed: 11477652]
48. Aslan S, Xu F, Wang PL et al. Estimation of labeling efficiency in pseudocontinuous arterial spin labeling. Magn Reson Med 2010; 63(3): 765–771. [PubMed: 20187183]
49. Attwell D, Laughlin SB. An energy budget for signaling in the grey matter of the brain. J Cereb Blood Flow Metab 2001; 21(10): 1133–1145. [PubMed: 11598490]
50. Mintun MA, Raichle ME, Kilbourn MR et al. A quantitative model for the in vivo assessment of drug binding sites with positron emission tomography. Ann Neurol 1984; 15(3): 217–227. [PubMed: 6609679]
51. Liu P, Xu F, Lu H. Test-retest reproducibility of a rapid method to measure brain oxygen metabolism. Magn Reson Med 2013; 69(3): 675–681. [PubMed: 22517498]
52. Liu P, Huang H, Rollins N et al. Quantitative assessment of global cerebral metabolic rate of oxygen (CMRO2) in neonates using MRI. NMR Biomed 2014; 27(3): 332–340. [PubMed: 24399806]
53. Lee H, Langham MC, Rodriguez-Soto AE et al. Multiplexed MRI methods for rapid estimation of global cerebral metabolic rate of oxygen consumption. Neuroimage 2017; 149: 393–403. [PubMed: 28179195]
54. Cho J, Kee Y, Spincemaille P et al. Cerebral metabolic rate of oxygen (CMRO2) mapping by combining quantitative susceptibility mapping (QSM) and quantitative blood oxygenation level-dependent imaging (qBOLD). Magn Reson Med 2018; 80(4): 1595–1604. [PubMed: 29516537]
55. Gauthier CJ, Hoge RD. A generalized procedure for calibrated MRI incorporating hyperoxia and hypercapnia. Hum Brain Mapp 2013; 34(5): 1053–1069. [PubMed: 23015481]
56. Ma Y, Sun H, Cho J et al. Cerebral OEF quantification: A comparison study between quantitative susceptibility mapping and dual-gas calibrated BOLD imaging. Magn Reson Med 2020; 83(1): 68–82. [PubMed: 31373088]

57. Fan AP, Benner T, Bolar DS et al. Phase-based regional oxygen metabolism (PROM) using MRI. Magn Reson Med 2012; 67(3): 669–678. [PubMed: 21713981]
58. Christen T, Bouzat P, Pannetier N et al. Tissue oxygen saturation mapping with magnetic resonance imaging. J Cereb Blood Flow Metab 2014; 34(9): 1550–1557. [PubMed: 25005878]
59. Tropp J, Lupo JM, Chen A et al. Multi-channel metabolic imaging, with SENSE reconstruction, of hyperpolarized [1-(13)C] pyruvate in a live rat at 3.0 tesla on a clinical MR scanner. J Magn Reson 2011; 208(1): 171–7. [PubMed: 21130012]
60. Brendel M, Deussing M, Blume T et al. Late-stage Anle138b treatment ameliorates tau pathology and metabolic decline in a mouse model of human Alzheimer's disease tau. Alzheimers Res Ther 2019; 11(1): 67. [PubMed: 31370885]
61. Adlimoghaddam A, Snow WM, Stortz G et al. Regional hypometabolism in the 3xTg mouse model of Alzheimer's disease. Neurobiol Dis 2019; 127: 264–277. [PubMed: 30878533]
62. Wells JA, Holmes HE, O'Callaghan JM et al. Increased cerebral vascular reactivity in the tau expressing rTg4510 mouse: evidence against the role of tau pathology to impair vascular health in Alzheimer's disease. J Cereb Blood Flow Metab 2015; 35(3): 359–362. [PubMed: 25515210]
63. Park L, Hochrainer K, Hattori Y et al. Tau induces PSD95-neuronal NOS uncoupling and neurovascular dysfunction independent of neurodegeneration. Nat Neurosci 2020; 23(9): 1079–1089. [PubMed: 32778793]
64. Yoshiyama Y, Higuchi M, Zhang B et al. Synapse loss and microglial activation precede tangles in a P301S tauopathy mouse model. Neuron 2007; 53(3): 337–351. [PubMed: 17270732]
65. Ramsden M, Kotilinek L, Forster C et al. Age-dependent neurofibrillary tangle formation, neuron loss, and memory impairment in a mouse model of human tauopathy (P301L). J Neurosci 2005; 25(46): 10637–10647. [PubMed: 16291936]
66. Jack CR, Knopman DS, Jagust WJ et al. Tracking pathophysiological processes in Alzheimer's disease: an updated hypothetical model of dynamic biomarkers. The Lancet Neurology 2013; 12(2): 207–216. [PubMed: 23332364]
67. Katzman R, Terry R, DeTeresa R et al. Clinical, pathological, and neurochemical changes in dementia: a subgroup with preserved mental status and numerous neocortical plaques. Ann Neurol 1988; 23(2): 138–144. [PubMed: 2897823]
68. Ibaraki M, Miura S, Shimosegawa E et al. Quantification of cerebral blood flow and oxygen metabolism with 3-dimensional PET and 15O: validation by comparison with 2-dimensional PET. J Nucl Med 2008; 49(1): 50–59. [PubMed: 18077532]
69. Krishnamurthy LC, Liu P, Ge Y et al. Vessel-specific quantification of blood oxygenation with T2-relaxation-under-phase-contrast MRI. Magn Reson Med 2014; 71(3): 978–989. [PubMed: 23568830]
70. Uwano I, Kudo K, Sato R et al. Noninvasive Assessment of Oxygen Extraction Fraction in Chronic Ischemia Using Quantitative Susceptibility Mapping at 7 Tesla. Stroke 2017; 48(8): 2136–2141. [PubMed: 28663515]
71. He X, Yablonskiy DA. Quantitative BOLD: mapping of human cerebral deoxygenated blood volume and oxygen extraction fraction: default state. Magn Reson Med 2007; 57(1): 115–126. [PubMed: 17191227]
72. Oshima T, Karasawa F, Okazaki Y et al. Effects of sevoflurane on cerebral blood flow and cerebral metabolic rate of oxygen in human beings: a comparison with isoflurane. Eur J Anaesthesiol 2003; 20(7): 543–7. [PubMed: 12884987]

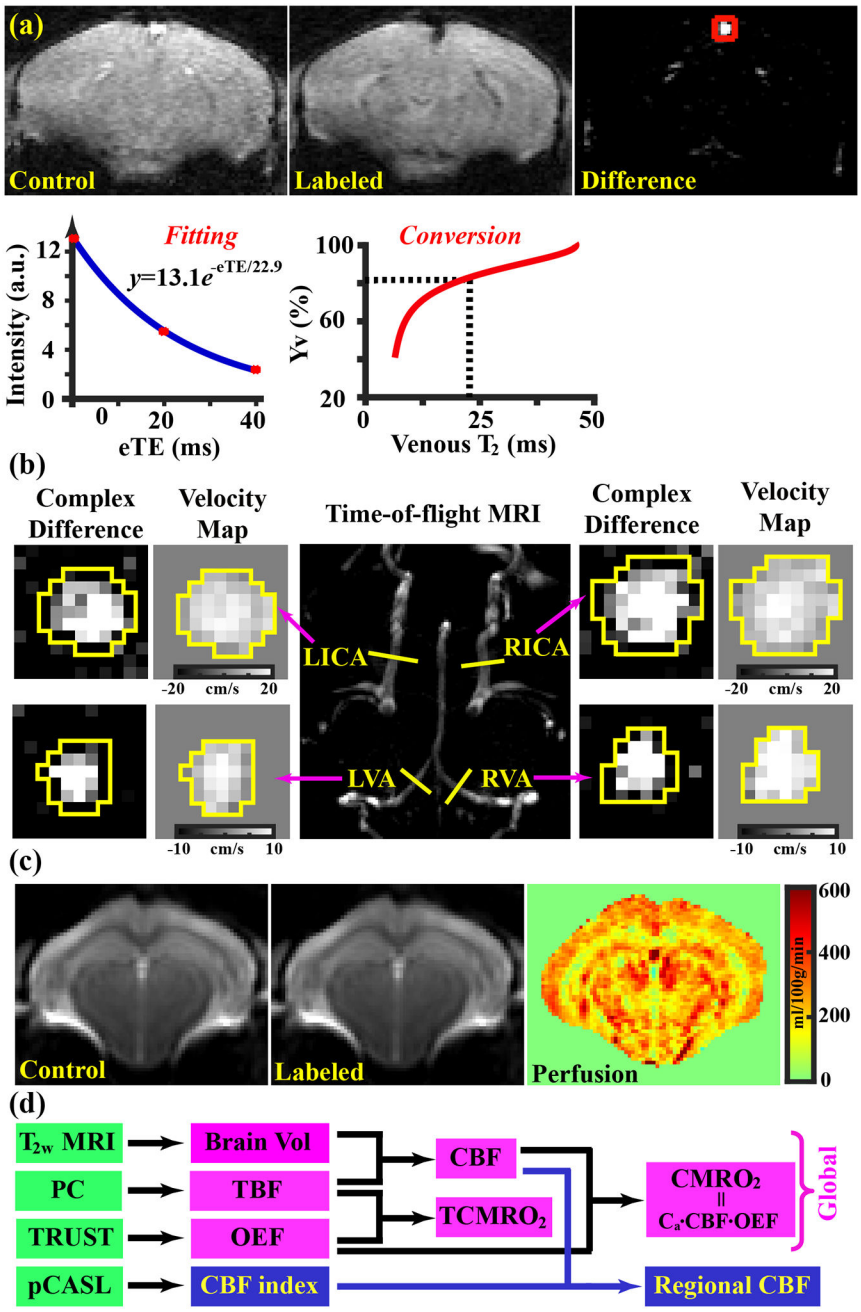

Figure 1:

Representative data of TRUST, PC, and pCASL MRI. (a) TRUST MRI. top row: pair-wise subtraction between control and labeled images yielded difference image with pure venous-blood signal (marked with red square); bottom row: venous-blood signal intensities were fitted into a monoexponential function to estimate venous T_2, which was then converted into Y_v value with an Hct-specific T_2-Y_v calibration plot. (b) PC MRI. Maximum intensity projection of time-of-flight (TOF) images (center column) was used for positioning. Complex-difference images and velocity maps of the four feeding arteries are shown in the left and right columns. (c) Control and labeled pCASL images as well as the perfusion

map from a representative slice. (d) schematic diagram to show global and regional measurements in the present study.

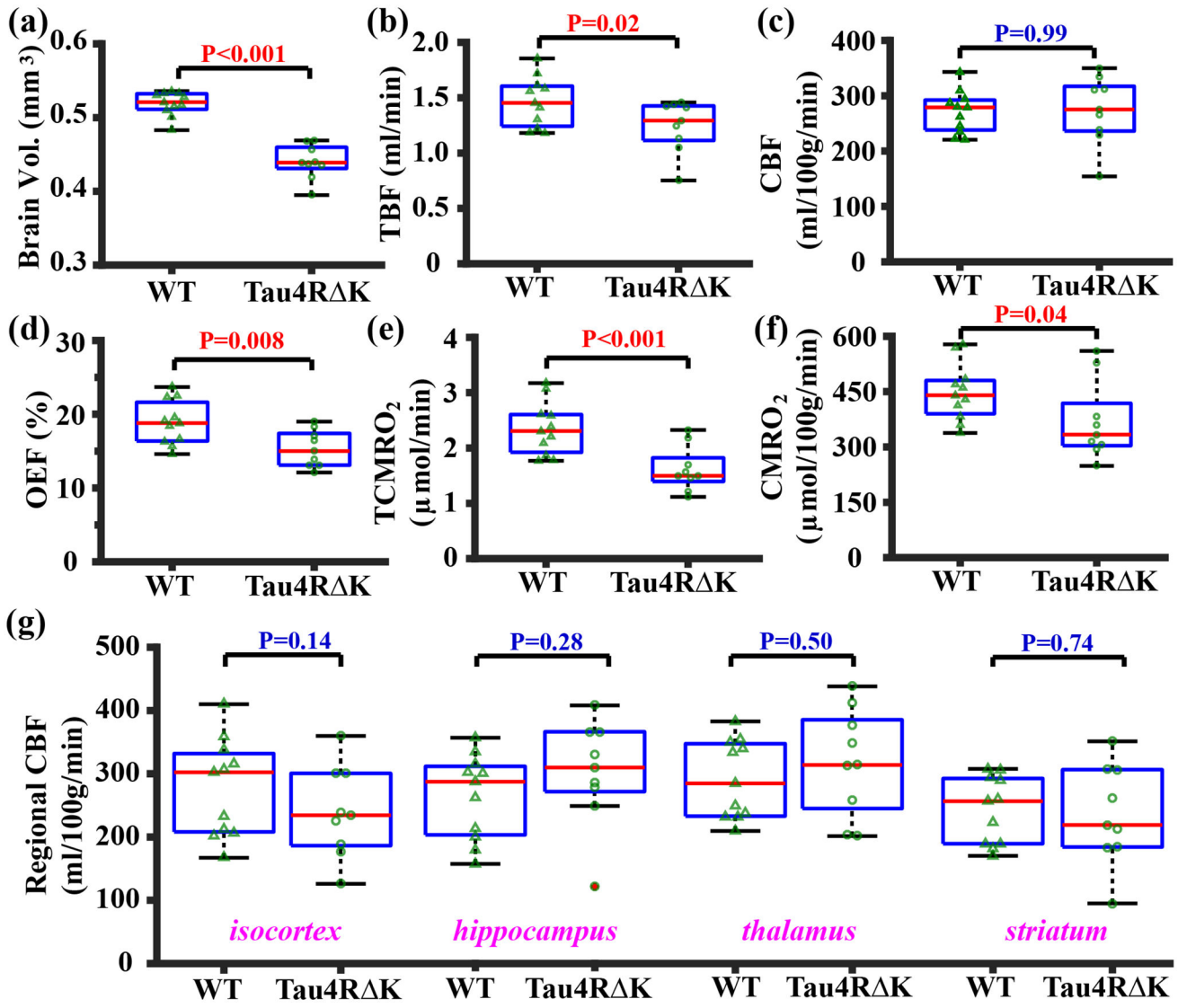

Figure 2:

Summary of MRI data in the Tau4RΔK mice. (a) brain volume, (b) TBF, (c) unit-mass CBF, (d) OEF, (e) $TCMRO_2$, (f) unit-mass $CMRO_2$, and (g) regional CBF in Tau4RΔK (N=9) and WT (N=11) mice shown with box plots. Triangles and circles overlaid on the box plots denote the measures in different mice of WT and Tau4RΔK groups, respectively. P-values correspond to the group effects in each measurement.

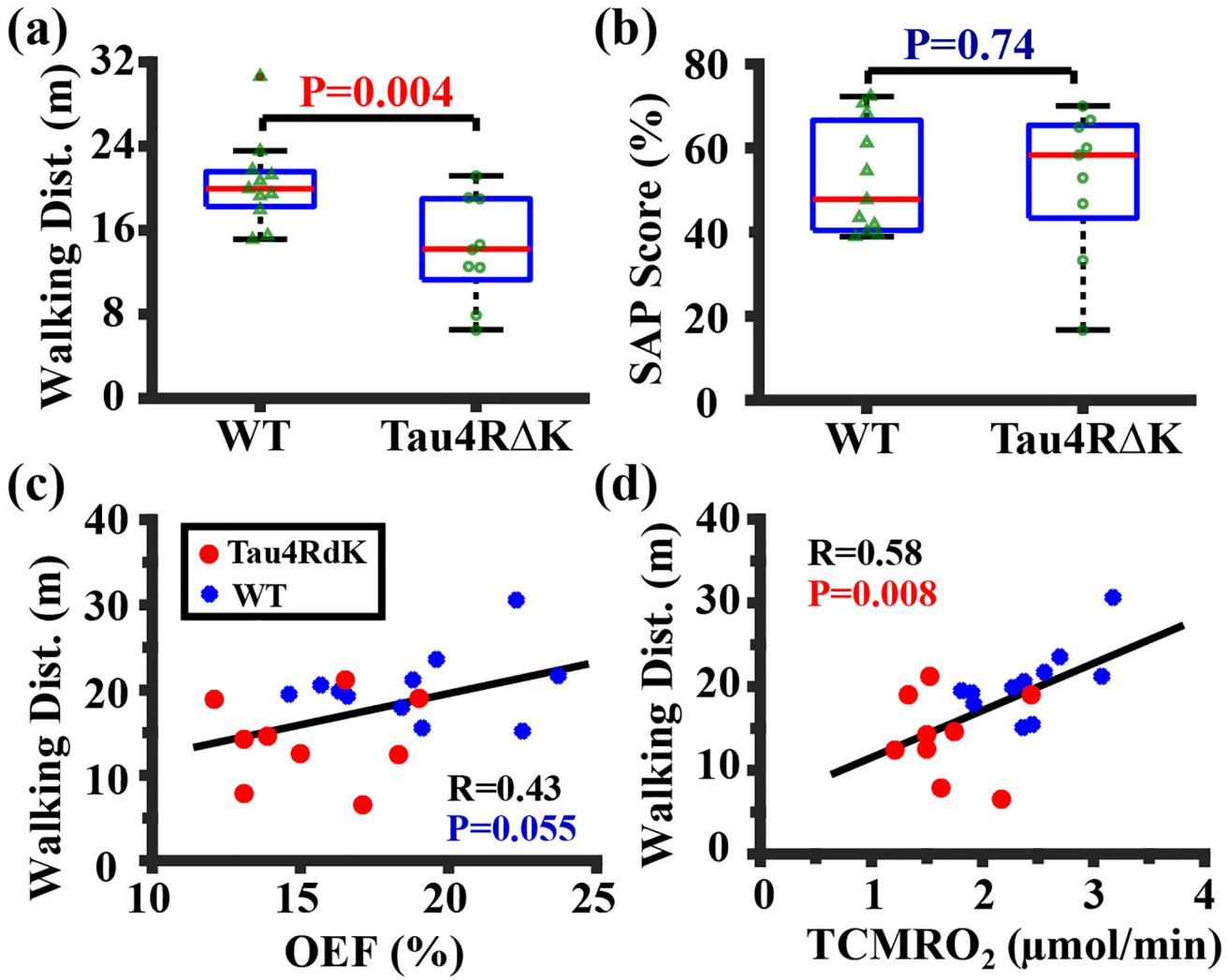

Figure 3:

Behavioral performance and its correlation with oxygen metabolism in the Tau4RΔK study. (a) Walking distance and (b) SAP score in Tau4RΔK (N=9) and WT (N=11) mice shown with box plots. (c) Correlation between walking distance and OEF. (d) Correlation between walking distance and $TCMRO_2$. Red and blue dots represented Tau4RΔK and WT mice, respectively.

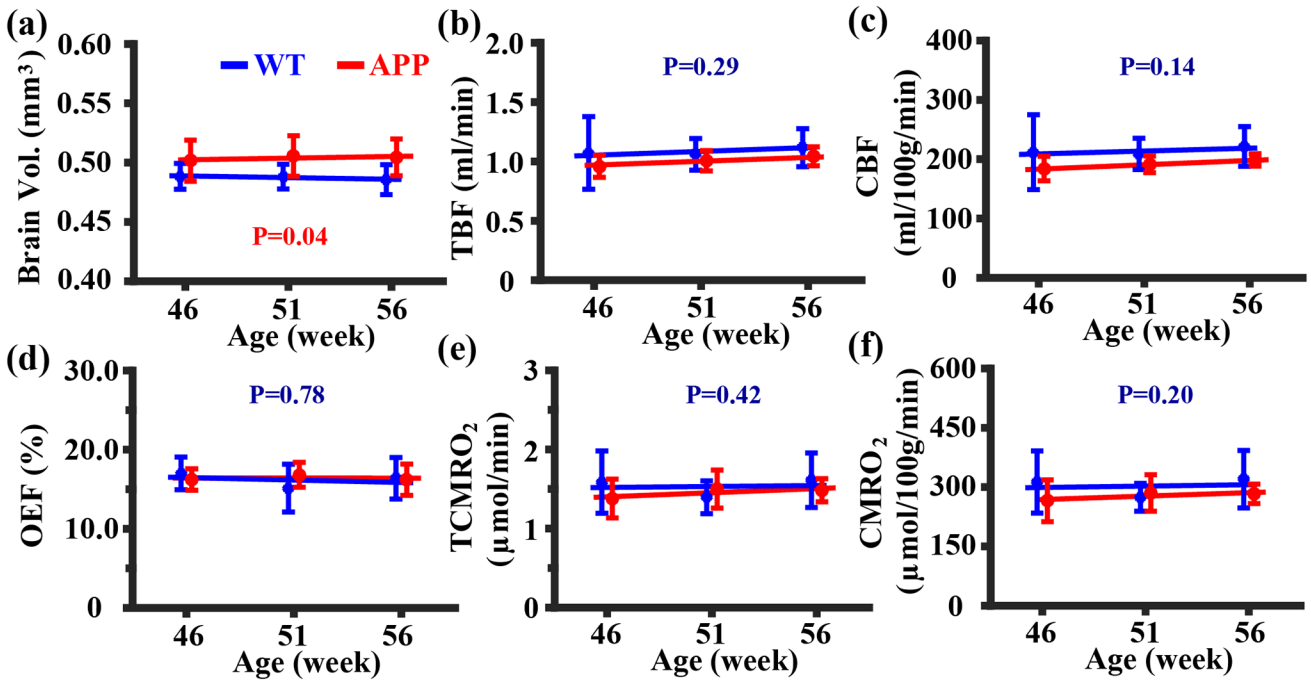

Figure 4:

Summary of MRI data in the APP study. (a) brain volume, (b) TBF, (c) CBF, (d) OEF, (e) $TCMRO_2$, and (f) $CMRO_2$ measurements in APP (N=5) and WT (N=5) mice were displayed for each time point. Errobar denotes the standard deviation across subjects. Solid lines represent fitted lines obtained from the linear mixed-effect model analyses, and P-values correspond to the group effects in each measurement.